Author(s): Heikkilä, Tero; Volovik, G. E.

Title: Nexus and Dirac lines in topological materials

Year: 2015

Version:

Please cite the original version:

Heikkilä, T., & Volovik, G. E. (2015). Nexus and Dirac lines in topological materials. New Journal of Physics, 17(September), Article 093019. https://doi.org/10.1088/1367-2630/17/9/093019

Nexus and Dirac lines in topological materials

2015 New J. Phys. 17 093019

(http://iopscience.iop.org/1367-2630/17/9/093019)

New Journal of Physics
The open access journal at the forefront of physics

Deutsche Physikalische Gesellschaft DPG
IOP Institute of Physics

Published in partnership with: Deutsche Physikalische Gesellschaft and the Institute of Physics

OPEN ACCESS

RECEIVED
8 June 2015

REVISED
6 August 2015

ACCEPTED FOR PUBLICATION
11 August 2015

PUBLISHED
11 September 2015

PAPER

Nexus and Dirac lines in topological materials

T T Heikkilä[1,4] and G E Volovik[2,3]

[1] University of Jyvaskyla, Department of Physics and Nanoscience Center, PO Box 35, FI-40014 University of Jyväskylä, Finland
[2] Low Temperature Laboratory, Aalto University, PO Box 15100, FI-00076 Aalto, Finland
[3] L. D. Landau Institute for Theoretical Physics, 117940 Moscow, Russia
[4] Author to whom any correspondence should be addressed.

E-mail: Tero.T.Heikkila@jyu.fi **and** volovik@boojum.hut.fi

Keywords: nexus, graphite, dirac lines

Abstract

We consider the Z_2 topology of the Dirac lines, i.e., lines of band contacts, on an example of graphite. Four lines—three with topological charge $N_1 = 1$ each and one with $N_1 = -1$—merge together near the H-point and annihilate due to summation law $1 + 1 + 1 - 1 = 0$. The merging point is similar to the real-space nexus, an analog of the Dirac monopole at which the Z_2 strings terminate.

1. Introduction

Dirac points in 2D systems and Dirac lines in 3D are examples of the exceptional points and lines of level crossing analyzed by von Neumann and Wigner [1]. They are typically protected by symmetry and are described by the Z_2 topological invariant (see [2]). Close to the 2D Dirac point with nontrivial topological charge N_1, the energy spectrum after deformation can be represented by the 2×2 matrix $H_{\rm Dirac} = c\,(\sigma_1 p_x \pm \sigma_2 p_y)$, where the Pauli matrices $\sigma_{1,2}$ describe the pseudo-spin induced in the vicinity of the level crossing. This gives rise to the conical spectrum near the Dirac point $E = E_0 \pm c|\mathbf{p}_\perp|$. For Dirac lines in 3D, the components p_x and p_y are in the transverse plane.

The Dirac Hamiltonian anticommutes with σ_3, which allows us to have the analytic form for the topological charge N_1, see e.g. review [3]:

$$N_1 = \mathbf{tr} \oint_C \frac{\mathrm{d}l}{4\pi \mathrm{i}} \cdot \left[\sigma_3 H^{-1}_{\rm Dirac}(\mathbf{p}) \partial_l H_{\rm Dirac}(\mathbf{p})\right]. \quad (1)$$

Here C is an infinitesimal contour in momentum space around the Dirac point or the Dirac line. The topological charge N_1 in equation (1) is integer: $N_1 = 1$ for sign $+$ and $N_1 = -1$ for sign $-$. However, the integer-valuedness emerges only in the vicinity of the Dirac point or line. In general, the summation rule is $1 + 1 = 2 \equiv 0$. This means that the Dirac line with $N_1 = 2$ can be continuously deformed to the trivial configuration.

In time reversal symmetric superconductors, due to chiral symmetry the Dirac lines may have zero energy and thus correspond to the nodal lines in the spectrum. Such lines exist in cuprate superconductors. According to the bulk-boundary correspondence the nodal lines may produce a dispersionless spectrum on the boundary —the flat band with zero energy [4–6]. If time reversal symmetry is violated (for example, by supercurrent), the Dirac line acquires a nonzero energy, a Fermi surface is formed, and the Dirac line lives inside the Fermi surface. In cuprate superconductors, the Fermi surfaces created by supercurrent around Abrikosov vortices give rise, at zero temperature, to the finite density of states proportional to $\sqrt{B}$, where B is the magnetic field [7].

Examples of semimetals with 2D Dirac points and 3D Dirac lines are provided by graphene and graphite, correspondingly. In these materials the spin–orbit interaction can be ignored, and one can consider them as spinless materials. In graphene there are two Dirac points in the Brillouin zone. If graphene is treated as spinless, one Dirac point has $N_1 = +1$ and another one has $N_1 = -1$ (for spinful electrons these are $N_1 = +2$ and $N_1 = -2$, correspondingly).

In rhombohedral graphite (ABCABC... stacking) two Dirac points of graphene layers generate two well-separated Dirac lines. Each has a form of a spiral and is characterized by the topological charge $N_1 = +1$ or $N_1 = -1$ [8, 9]. These Dirac lines have nonzero energy and live inside the chains of the hole and electron Fermi

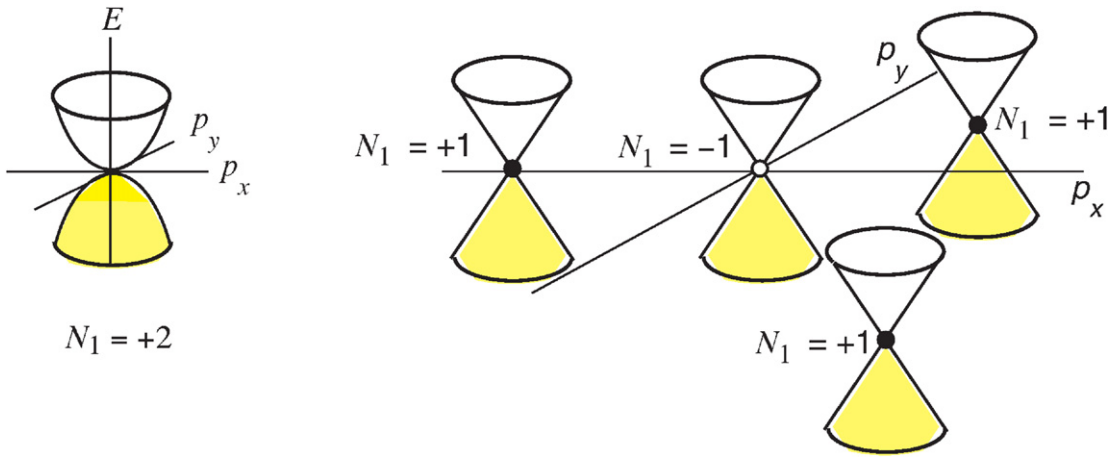

Figure 1. Z_2-topology of Dirac points in bilayer graphene. Left: dirac point with quadratic spectrum characterized by topological invariant $N_1 = 2$. Since the topological invariant is trivial in Z_2 topology, such a spectrum is unstable towards the gap formation, or to splitting. Right: splitting to topologically stable Dirac points due to trigonal warping.

surfaces, discussed by McClure (see figure 2 in [10]). The projection of the spiral to the top or bottom surface of graphite determines the boundary of the (approximate) surface flat band [8, 9]. This flattening of the spectrum has been recently observed in epitaxial rhombohedral multilayer graphene[11].

2. Bilayer graphene

In Bernal graphite (ABAB... stacking) the geometry of the Dirac lines is essentially different from rhombohedral graphite, because Bernal graphite is the 3D extension of bilayer graphene with AB stacking. Let us hence start by describing the bilayer graphene with AB stacking.

Since in each graphene layer the topological charges are $N_1 = +1$ and $N_1 = -1$ in the two valleys, in bilayer graphene the charges are summed up giving rise to trivial topological charges $N_1 = +2 \equiv 0$ and $N_1 = -2 \equiv 0$. Interaction between the layers may lead to several possible scenarios of the geometry of the fermionic spectrum in bilayer graphene:

(i) If there is some special symmetry, such as the fundamental Lorentz invariance, one obtains a doubly degenerate conical spectrum. However, in bilayer graphene there is no symmetry which could support such a scenario.

(ii) The topological charge $N_1 = 2$ gives rise to the Dirac fermions with parabolic energy spectrum near the Dirac point, $E = E_0 \pm \mathbf{p}_\perp^2/2m$ (figure 1(left)). Such a spectrum belongs to the trivial element of the group Z_2, that is why the neglected hopping elements destroy the parabolic spectrum. The Dirac point disappears, and finite gap (the Dirac mass) emerges.

(iii) The Dirac point with $N_1 = +2$ splits into two Dirac points, each with $N_1 = +1$ and with conical spectrum (see [12] for the relativistic 3+1 system). Such splitting, however, violates the hexagonal symmetry of graphene.

(iv) The splitting of the $N_1 = +2$ Dirac point, which is consistent with the hexagonal symmetry, is in figure 1(right). The $N_1 = +2$ Dirac point splits into four Dirac conical points: the central Dirac point has $N_1 = -1$, while three others with $N_1 = +1$ each are connected by the C_3 symmetry, see figure 1(right). This is called the trigonal warping. The topological charges $N_1 = \pm 1$ belong to the nontrivial element of the group Z_2. That is why each Dirac point is topologically stable and is not destroyed by addition of the neglected hopping elements, if they obey the time reversal and sublattice symmetry.

The bilayer graphene chooses the scenario (iv) with the trigonal warping [13, 14], which prohibits the annihilation of the Dirac point due to splitting into the topologically stable Dirac points with $N_1 = \pm 1$. Altogether the Brillouin zone of the bilayer graphene contains 8 Dirac conical points.

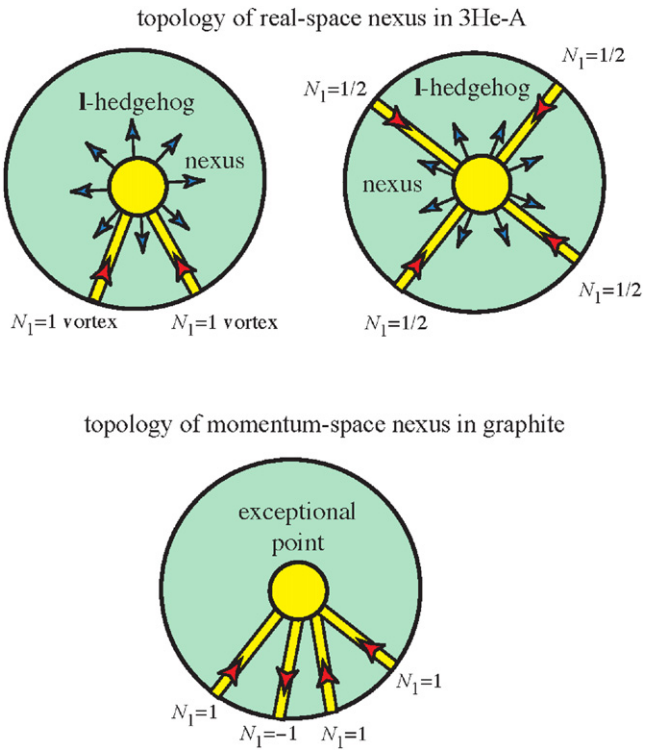

Figure 2. Real-space and momentum space nexus. Top left: real-space nexus in the dipole locked superfluid ^{3}He-A, where vortices are described by Z_2-topology. Two vortices, with $N_1 = 1$ each, merge together at the hedgehog in the field of the orbital momentum vector $\hat{\mathbf{l}}$ and annihilate each other since $N_1 = 2 \equiv 0$. Top right: real-space nexus in the dipole unlocked superfluid ^{3}He-A, where vortices are described by Z_4-topology. Four half-quantum vortices, with $N_1 = 1/2$ each, merge together at the hedgehog and annihilate each other. Bottom: illustration of the topology of the momentum-space nexus in graphite. Dirac lines obey the Z_2-topology. Four Dirac lines, with $N_1 = +1$, $N_1 = +1$, $N_1 = +1$ and $N_1 = -1$, merge together at an exceptional point of the spectrum and annihilate each other, because $N_1 = 1 + 1 + 1 - 1 = 2 \equiv 0$.

3. From topology of bilayer graphene to Bernal graphite

The trigonal warping also stabilizes the Dirac lines in the Bernal graphite (ABAB... stacking). Altogether the Brillouin zone of the Bernal graphite contains 8 Dirac lines [15, 16], which originate from 8 Dirac conical points of bilayer graphene. These Dirac lines have finite energy and live inside the Fermi surface of graphite.

However, the topologically stable Dirac lines appear only in a certain region of momenta p_z. Outside that region the scenario (ii) without the Dirac lines takes place. This means that there exists an exceptional point in the spectrum, at which four topologically stable Dirac lines merge together and annihilate each other [15, 16]. Such a point is a direct analog of the nexus, a point in the real space where the Z_2 or Z_4 topological defects merge and annihilate each other, see figure 2(top) [18].

Let us find this exceptional point. According to D_{6h} symmetry of graphite, the Dirac lines are situated in the vertical mirror planes, and thus the exceptional point is on the H-K-H line in the Brillouin zone at $p_z = P^*$.

The Hamiltonian of Bernal graphite is a 3D extension of the 2D Hamiltonian describing bilayer graphene:

$$H = \begin{pmatrix} \Delta & v_F p e^{-i\phi} & \gamma_4 \Gamma(p_z) v_F p e^{i\phi} & -2\gamma_1 \Gamma(p_z) \\ v_F p e^{i\phi} & \gamma_2(p_z) & 2\gamma_3 \Gamma(p_z) v_F p e^{-i\phi} & \gamma_4 \Gamma(p_z) v_F p e^{i\phi} \\ \gamma_4 \Gamma(p_z) v_F p e^{-i\phi} & 2\gamma_3 \Gamma(p_z) v_F p e^{i\phi} & \gamma_2(p_z) & v_F p e^{-i\phi} \\ -2\gamma_1 \Gamma(p_z) & \gamma_4 \Gamma(p_z) v_F p e^{-i\phi} & v_F p e^{i\phi} & \Delta \end{pmatrix}. \quad (2)$$

This corresponds to a rotated version of that written in [10] (we write the Hamiltonian in a basis spanned by the two layers $\times$sublattice points, whereas [10] writes it in the eigenbasis defined by the strongest interlayer couplings), but we assume that the intralayer coupling γ_0 dominates over the other terms, and therefore also make the $\sigma \cdot p$ approximation for each layer. Here $p e^{i\phi} = p_x + i p_y$; $\Gamma(p_z) = \cos((\pi/2a)p_z)$, where a is the distance between the K-point and H-point in the Brillouin zone of graphite and $p_z = 0$ at the K-point so that $\Gamma(K) = 1$ and $\Gamma(H) = 0$. The function $\gamma_2(p_z) = \gamma_2 \Gamma^2(p_z)/2$ describes the coupling across two layers and Δ denotes the locally broken A-B sublattice symmetry, which still preserves the global A-B symmetry. The

coefficients $\gamma_{3,4}$ are related to the original tight-binding coefficients [10] $\tilde{\gamma}_{3,4}$ via $\gamma_{3,4} = \tilde{\gamma}_{3,4}/\gamma_0$. In graphite, $\gamma_3 \approx 0.1$ and $\gamma_4 \approx 0.01$ [17]. We neglect spin–orbit coupling and below we set $v_F = 1$ for simplicity.

Hamiltonian (2) is invariant under time reversal symmetry (complex conjugation) combined with reflection from plane $p_y = 0$ ($\phi \to -\phi$). This symmetry supports the Z_2 topology of Dirac points in graphene (figure 1(right)) and Dirac lines in graphite.

4. Point of merging of Dirac lines

Since the merging point P^* is on the H-K-H line, we consider the Hamiltonian at $p = 0$ which has the following form (we consider only the traceless part):

$$\tilde{H}\left(p = 0, p_z\right) = H\left(p = 0, p_z\right) - \frac{1}{4}\,\mathbf{Tr}\, H\left(p = 0, p_z\right)$$
$$= \begin{pmatrix} f\left(p_z\right) & 0 & 0 & -2g\left(p_z\right) \\ 0 & -f\left(p_z\right) & 0 & 0 \\ 0 & 0 & -f\left(p_z\right) & 0 \\ -2g\left(p_z\right) & 0 & 0 & f\left(p_z\right) \end{pmatrix},$$
$$f\left(p_z\right) = \frac{1}{2}\left(\Delta - \gamma_2\left(p_z\right)\right), \quad g\left(p_z\right) = \gamma_1 \Gamma\left(p_z\right). \tag{3}$$

This can be rewritten in terms of the Pauli matrices σ_i and τ_i:

$$\tilde{H}\left(p = 0, p_z\right) = f\left(p_z\right)\tau_3\sigma_3 + g\left(p_z\right)(\tau_2\sigma_2 - \tau_1\sigma_1). \tag{4}$$

Let us introduce new matrices $\tilde{\tau}_3 = -\tau_3$, $\tilde{\tau}_1 = -\tau_1$, $\tilde{\tau}_2 = \tau_2$ and the 'total spin' $\mathbf{J} = \frac{1}{2}(\boldsymbol{\sigma} + \boldsymbol{\tau})$:

$$\tilde{H}\left(p = 0, p_z\right) = -\left(f\left(p_z\right) + g\left(p_z\right)\right)\tilde{\tau}_3\sigma_3 + g\left(p_z\right)\boldsymbol{\sigma}\cdot\tilde{\boldsymbol{\tau}}, \tag{5}$$

$$\boldsymbol{\sigma}\cdot\tilde{\boldsymbol{\tau}} = 2J(J+1) - 3\ , \quad \tilde{\tau}_3\sigma_3 = 2J_3^2 - 1. \tag{6}$$

The Hamiltonian at $p = 0$ can be expressed in terms of quantum numbers J and J_3:

$$\tilde{H}(p = 0) = -\left(f\left(p_z\right) + g\left(p_z\right)\right)\left(2J_3^2 - 1\right) + g\left(p_z\right)(2J(J+1) - 3). \tag{7}$$

The exceptional point $p_z = P^*$ is at $f(p_z) + g(p_z) = 0$, where three branches of the spectrum with $J = 1$ are degenerate. Its position is determined by equation

$$\Delta - \gamma_2\left(p_z\right) + 2\gamma_1\Gamma\left(p_z\right) = 0. \tag{8}$$

In other notations this is the known equation for the exceptional point in graphite, see e.g. [16]. It is situated in the vicinity of the H-point. Away from this point, two branches with $J_3 = \pm 1$ remain degenerate for all p_z. Close to the exceptional point

$$\tilde{H}(p = 0, J = 1) \approx -\lambda\left(p_z - P^*\right)\left(2J_3^2 - 1\right) + g\left(P^*\right), \tag{9}$$

where $\lambda = f'(P^*) + g'(P^*)$.

The exceptional point P^* is the merging point of four Dirac lines living in the symmetry planes at $p_z < P^*$. At $p_H > p_z > P^*$ the spectrum remains degenerate: the branches with $J_3 = +1$ and $J_3 = -1$ have the same energy. But these are the band contact lines rather than the Dirac lines: the branches have the same sign of energy counted from the line position, as distinct from $p_z < P^*$, where the touching branches have energies with opposite sign, which is the characteristics of a Dirac line (see figure 3). This means that at $p_z = P^*$ a band inversion occurs. The band inversion simultaneously happens for the branch with quantum numbers $J = 1$ and $J_3 = 0$.

5. 2D Dirac fermions at H-point

To see that the topology at $p_H > p_z > P^*$ is trivial, let us consider the $p_{x/y}$ plane containing the H-point. Since $\Gamma(p_H) = 0$, the Hamiltonian at the plane $p_z = p_H$ is

$$\tilde{H}(p, H) = \frac{1}{2}\left(\Delta - \gamma_2\left(p_H\right)\right)\tau_3\sigma_3 + p_x\sigma_1 + p_y\sigma_2. \tag{10}$$

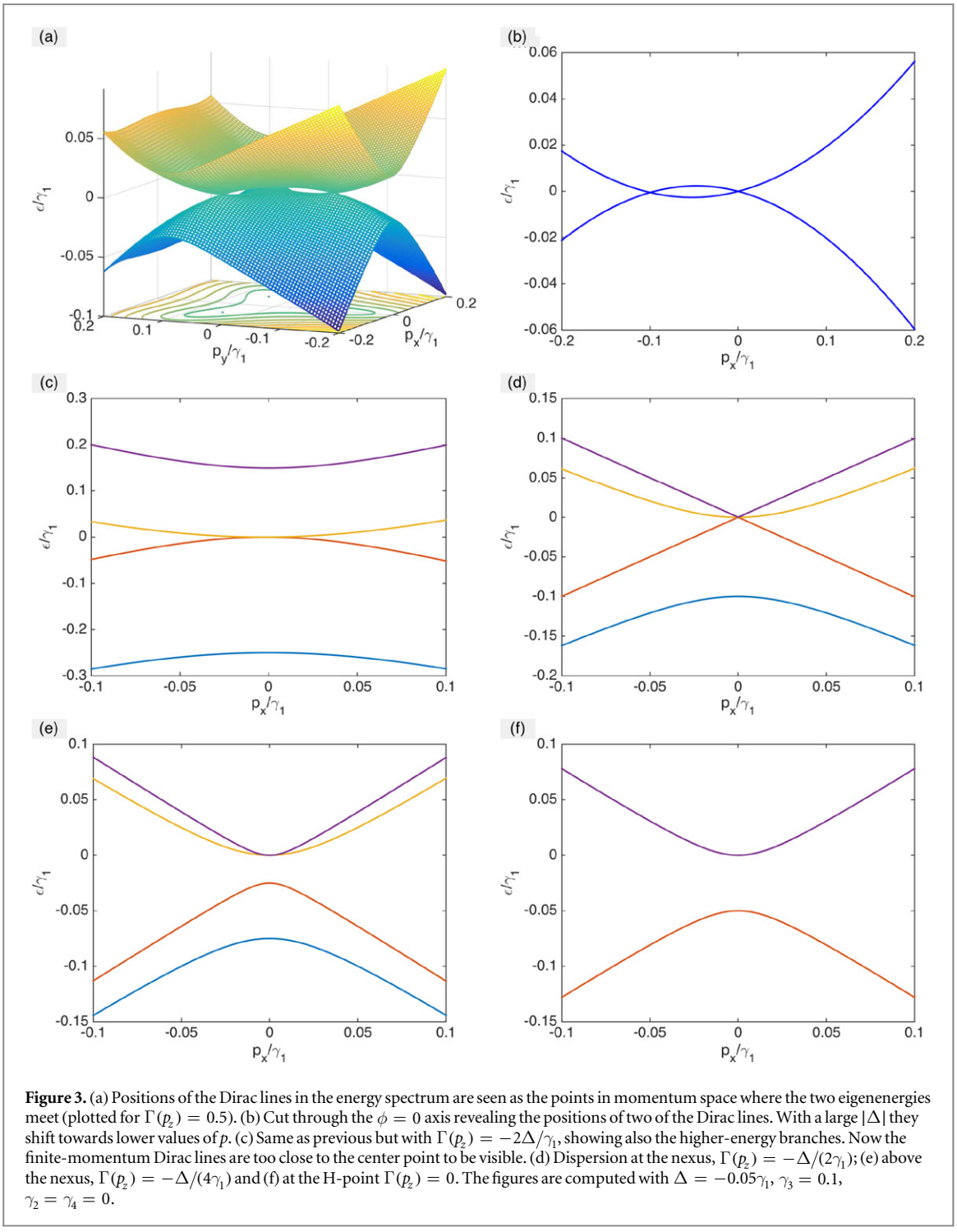

Figure 3. (a) Positions of the Dirac lines in the energy spectrum are seen as the points in momentum space where the two eigenenergies meet (plotted for $\Gamma(p_z) = 0.5$). (b) Cut through the $\phi = 0$ axis revealing the positions of two of the Dirac lines. With a large $|\Delta|$ they shift towards lower values of p. (c) Same as previous but with $\Gamma(p_z) = -2\Delta/\gamma_1$, showing also the higher-energy branches. Now the finite-momentum Dirac lines are too close to the center point to be visible. (d) Dispersion at the nexus, $\Gamma(p_z) = -\Delta/(2\gamma_1)$; (e) above the nexus, $\Gamma(p_z) = -\Delta/(4\gamma_1)$ and (f) at the H-point $\Gamma(p_z) = 0$. The figures are computed with $\Delta = -0.05\gamma_1$, $\gamma_3 = 0.1$, $\gamma_2 = \gamma_4 = 0$.

It represents two copies of massive 2D fermions with Dirac spectrum:

$$\tilde{E}(p) = \pm\sqrt{M^2 + p^2}\,, \quad M = \frac{1}{2}\Big(\Delta - \gamma_2\big(p_H\big)\Big). \tag{11}$$

and thus two doubly degenerate branches. In addition to the contact line of $J_z = \pm 1$ branches, the other two branches, $J = 1$, $J_3 = 0$ and $J = J_3 = 0$, contact each other. The Hamiltonian (10) has trivial N_1 topology. Due to continuity, the topology in the plane slightly below the H-point is also trivial. This demonstrates that at $p_H > p_z > P^*$ there are no Dirac lines. Instead there are band-contact lines, with trivial topological charge $N_1 = 0$. Thus the exceptional point P^* is the point of merging of four Dirac lines.

6. Finite-energy Dirac lines

Let us consider the occurrence of the Dirac lines at a finite energy. For simplicity, we neglect $\gamma_2(p_z)$ and γ_4, as they do not change the qualitative behavior of the Dirac lines close to the nexus. In this case, the characteristic equation for the bulk spectrum reads

$$\left(p^2 + (\Delta - \epsilon)\epsilon\right)^2 + \left(-4p^3\gamma_3^2(\Delta - \epsilon)^2 - 4\gamma_1^2\epsilon^2 + 8p^3\gamma_1\gamma_3\cos(3\phi)\right)\Gamma^2\left(p_z\right) + 16p^2\gamma_1^2\gamma_3^2\Gamma\left(p_z\right)^4 = 0. \tag{12}$$

This has four solutions for ϵ. Let us analyze the solutions for three cases: (a) $|p_z| \ll P^*$, (b) $|p_z| = P^*$, and (c), $p_H \geqslant |p_z| > P^*$. The relevant eigensolutions for a specific set of parameters in the three cases are plotted in figure 3.

For region (a), there are two eigenenergies $\epsilon \approx \pm\gamma_1\Gamma(p_z)$, and two closer to zero. The latter two are plotted in figures 3(a), (b) for a fixed $\Gamma(p_z)$. Two low-energy solutions touch at specific points in the transverse momentum direction, either at $p = 0$ and close to $\cos(3\phi) = -1$, $p = p_0 = 4\gamma_1\gamma_3\Gamma^2(p_z)$, which is the exact position of the Dirac line for $\Delta = 0$. For small Δ, the Dirac lines at finite momentum obtain a finite energy $\epsilon = \Delta[1 - 1/(1 + 4\gamma_3^2\Delta\Gamma^2(p_z))]$ and slightly shift the line away from $p = p_0$. The Dirac line character however persists. Figure 3(c) shows all four eigenenergies in region (a). Here the splitting of the two low-energy lines is not visible as they are quite close to each other.

For $p_z = P^*$, the four solutions are plotted in figure 3(d). For low Δ and p, the energies are given by

$$\epsilon_{1,2} = \Delta \pm \sqrt{\Delta^2 + p^2}\,,\ \epsilon_{3,4} = \pm p. \tag{13}$$

There are hence two gapped and quadratic and two gapless linear branches, and three of them meet at $\epsilon = p = 0$.

Above the nexus (region (c)), we may first set $\Gamma(p_z) = 0$, i.e., consider the H point. There, the finite-energy solutions are given by (shifted by a constant energy from equation (11))

$$\epsilon_{a,b} = \frac{1}{2}\left(\Delta \pm \sqrt{4p^2 + \Delta^2}\right), \tag{14}$$

The energies, plotted in figure 3(f), are doubly degenerate, but the degeneracy is lifted for a finite $\Gamma(p_z)$, yielding two pairs of quadratic branches, the gap depending on the precise value of $\Gamma(p_z)$. The lifting of this degeneracy is shown in figure 3(e).

7. Nexus

In the real space, the nexus is a kind of a Dirac monopole that terminates cosmic strings (the so-called Z-string in the Standard Model) [19]. In chiral superfluid ^{3}He-A the nexus is a hedgehog which terminates vortices with the Z_2 or Z_4 topology (figure 17.3 in the book [18] and figure 2(top)). In the dipole-locked ^{3}He-A the homotopy group for vortices is Z_2. That is why two vortices can terminate at the hedgehog in the field of the orbital momentum vector $\hat{\mathbf{l}}$, which is the analog of the Dirac magnetic monopole.

In the same manner the Dirac lines can be described by the Z_2 group, and if so, they may terminate on a Dirac monopole in some field. If the invariant N_1 belongs to the Z_2 group, which means that $N_1 = 2$ and $N_1 = 0$ are equivalent, then by some transformation of hopping elements the line described by even $N_1 = 2k$ can disappear. The lines with $N_1 = \pm 1$ are stable. But when four such lines meet each other, their total charge is even, and thus they may annihilate each other. This also happens, since at $p_z > P^*$ the band contact lines are topologically trivial, $N_1 = 0$.

So, the point $p_z = P^*$ represents the nexus in momentum space, see figure 2(bottom). It is distinct from the 3D Weyl point in momentum space, which also represents the momentum-space analog of a Dirac monopole. Such a monopole contains the Dirac string: a singularity in the Berry phase which terminates at the monopole, see figure 11.4 in [18]. But this string is not observable.

8. Conclusion

The Dirac lines are suggested to exist in different semimetals [20–26]. The materials with Dirac lines are important, because they may have an (approximate) flat band on the boundary or at the interface between materials with different topological properties. The high density of states in the flat band provides a possible route to room-temperature superconductivity [27].

However, the Bernal graphite is a very instructive example. Its spectrum demonstrates the possible interplay of several relevant topological invariants. One of them characterizes the local line element as in [2]. Another one

is the global invariant, which characterizes for example the closed nodal ring as a whole: it is the same invariant which characterizes the 3D Dirac or Weyl point obtained by shrinking the nodal ring. There are also the topological invariants that characterize the Fermi surface(s). These include the local invariant of the Fermi surface [18] and the topology of the shape of the Fermi surface [28]. All this may combine to produce exotic topological patterns. The interplay of Weyl point and Fermi surface topologies with exchange of the Berry flux, when two Fermi surfaces contact each other, have been discussed in [26, 29]. The Bernal graphite provides an example of the interplay of Dirac lines in the mirror planes, an exceptional point (nexus), and Fermi surfaces with touching points between electron and hole pockets, see [15, 16].

Acknowledgments

This work was supported by the Academy of Finland through its Center of Excellence program and by the European Research Council (Grant No. 240362-Heattronics).

References

[1] von Neumann J and Wigner E P 1929 Über das Verhalten von Eigenwerten bei adiabatischen Prozessen *Phys. Zeit.* **30** 467–70
[2] Hořava P 2005 Stability of Fermi surfaces and K-theory *Phys. Rev. Lett.* **95** 016405
[3] Volovik G E 2013 The topology of quantum vacuum *Lecture Notes Phys.* **870** 343–83
[4] Ryu S and Hatsugai Y 2002 Topological origin of zero-energy edge states in particle-hole symmetric systems *Phys. Rev. Lett.* **89** 077002
[5] Schnyder A P and Ryu S 2011 Topological phases and flat surface bands in superconductors without inversion symmetry *Phys. Rev.* B **84** 060504(R)
[6] Schnyder A P and Brydon P M R 2015 Topological surface states in nodal superconductors *J. Phys.: Condens. Matter* **27** 243201
[7] Volovik G E 1993 Superconductivity with lines of gap nodes: density of states in the vortex *JETP Lett.* **58** 469–73
[8] Heikkilä T T and Volovik G E 2011 Dimensional crossover in topological matter: evolution of the multiple Dirac point in the layered system to the flat band on the surface *Pis'ma ZhETF* **93** 63–68
Heikkilä T T and Volovik G E 2011 *JETP Lett.* **93** 59–65
Heikkilä T T and Volovik G E 2010 arXiv:1011.4185
[9] Heikkilä T T, Kopnin N B and Volovik G E 2011 Flat bands in topological media *Pis'ma ZhETF* **94** 252– 258
Heikkilä T T, Kopnin N B and Volovik G E 2011 *JETP Lett.* **94** 233–9
Heikkilä T T, Kopnin N B and Volovik G E 2010 arXiv:1012.0905
[10] McClure J W 1957 Band structure of graphite and de Haas-van Alphen effect *Phys. Rev.* **108** 612–8
[11] Pierucci D *et al* 2015 Evidence for flat bands near the Fermi level in epitaxial rhombohedral multilayer graphene *ACS Nano* **9** 5432
[12] Klinkhamer F R and Volovik G E 2005 Emergent CPT violation from the splitting of Fermi points *Int. J. Mod. Phys.* A **20** 2795–812
Klinkhamer F R and Volovik G E 2004 arXiv:hep-th/0403037
[13] McCann E and Fal'ko V I 2006 Landau-level degeneracy and quantum Hall effect in a graphite bilayer *Phys. Rev. Lett.* **96** 086805
[14] Koshino M and Ando T 2006 Transport in bilayer graphene: Calculations within a self-consistent Born approximation *Phys. Rev.* B **73** 245403
[15] Mikitik G P and Sharlai Yu V 2006 Band-contact lines in the electron energy spectrum of graphite *Phys. Rev.* B **73** 235112
[16] Mikitik G P and Sharlai Yu V 2008 The Berry phase in graphene and graphite multilayers *Low Temp. Phys.* **34** 794–780
[17] Castro Neto A H, Guinea F, Peres N M R, Novoselov K S and Geim A K 2009 The electronic properties of graphene *Rev. Mod. Phys.* **81** 109
[18] Volovik G E 2003 *The Universe in a Helium Droplet* (Oxford: Oxford University Press)
[19] Cornwall J M 1999 Center vortices, nexuses, and the Georgi-Glashow model *Phys. Rev.* D **59** 125015
[20] Weng H, Liang Y, Xu Q, Rui Y, Fang Z and Xi Dai Y 2015 Kawazoe, Topological node-line semimetal in three dimensional graphene networks *Phys. Rev.* B **92** 045108
[21] Xie L S, Schoop L M, Seibel E M, Gibson Q D, Xie W and Cava R J 2015 Potential ring of Dirac nodes in a new polymorph of Ca_3P_2 *APL Mater.* **3** 083602
[22] Kim Y, Wieder B J, Kane C L and Rappe A M 2015 Dirac line nodes in inversion symmetric crystals *Phys. Rev. Lett.* **115** 036806
[23] Rui Y, Weng H, Fang Z, Dai X and Hu X 2015 Topological node-line semimetal and Dirac semimetal state in antiperovskite Cu_3 PdN *Phys. Rev. Lett.* **115** 036807
[24] Mullen K, Uchoa B and Glatzhofer D T 2015 Line of Dirac Nodes in Hyperhoneycomb Lattices *Phys. Rev. Lett.* **115** 026403
[25] Fang C, Chen Y, Kee H-Y and Fu L 2015 Topological nodal line semimetals with and without spin–orbital coupling *Phys. Rev.* B **92** 081201
[26] Gosalbez-Martinez D, Souza I and Vanderbilt D 2015 Chiral degeneracies and Fermi-surface Chern numbers in bcc Fe *Phys. Rev.* B **92** 085138
[27] Heikkilä T T and Volovik G E 2015 Flat bands as a route to high-temperature superconductivity in graphite (arXiv:1504.05824)
[28] Novikov S P and Maltsev A Ya 1998 Topological phenomena in normal metals *Phys.—Usp.* **41** 231–9
[29] Klinkhamer F R and Volovik G E 2005 Emergent CPT violation from the splitting of Fermi points Int. J *Mod. Phys.* A **20** 2795–812